ADVANCED FUNCTIONAL MATERIALS
www.afm-journal.de

Boosting OECT Performance with PEGylated Gold Nanoparticles in Hydrophobic Channels

Po Yuen Ho, Oliver Ditzer, Ali Solgi, Haoran Zhang, Ronja Thümmler, Mahmoud Al-Hussein, Hans Kleemann, Ningwei Sun, and Franziska S.-C. Lissel**

Organic electrochemical transistors (OECTs) require organic mixed ion-electron conductors (OMIECs) (i.e., hydrophilic materials supporting electron and ion transportation) as active materials. However, high-performance OMIECs grafted with hydrophilic side chains are difficult to synthesize and purify, and often suffer from swelling during operation. In contrast, the synthetic pathways toward a broad range of hydrophobic polymeric semiconductors used in classic organic-field-effect transistors are well established, and several are even commercially available. Yet, these hydrophobic materials do not intrinsically support ionic transport, limiting their application in OECTs. Here, poly(ethyleneglycol) (PEG)-coated gold nanoparticles (AuNP) are incorporated into conventional hydrophobic polymeric semiconductors like poly-3-hexylthiophene (P3HT), improving not only ionic but also electronic transport. The hydrophilic AuNPs modify P3HT crystallite orientation, shorten lamellar and π–π distances, and create pathways for ion penetration, as evidenced by GIWAXS and AFM studies. With 5 wt% AuNP loading, OECTs achieve μC^* of 98 F cm^{-1} V^{-1} s^{-1}, comparable to hydrophilic materials. The strategy also works for other polymer systems, offering a facile method to utilize hydrophobic materials in OECTs and boost their performance.

1. Introduction

Organic electrochemical transistors (OECTs) are promising candidates for applications such as physiological signal monitoring[1,2] and neuromorphic computing.[3–7] Unlike conventional organic field-effect transistors (OFETs), which rely on the formation of a conductive channel at the dielectric/semiconductor interface, OECTs allow for a volumetric doping/dedoping of the channel by ion penetration. To achieve this, OECTs rely on organic mixed ion-electron conductors (OMIECs) as active materials. OMIECs not only facilitate electron transport but also interact efficiently with electrolytic ions. The OECT figure of merit, μC^*, highlights the critical influence of two major factors: μ, which governs electronic transport property, and C^*, which governs ionic interaction capability. This results in much higher transconductance compared to OFETs,[8] making OECTs suitable for recording weak biological signals.

Poly(3,4-ethylenedioxythiophene) poly(styrene sulfonate) (PEDOT:PSS) is an extensively studied OMIEC among others due to its satisfying OECT performance and commercial availability. However, PEDOT:PSS operates in depletion mode, necessitating positive gate voltage to turn off the transistor, which complicates operation and potentially increases power consumption. To increase power efficiency and long-term stability, considerable effort has been directed toward enabling PEDOT:PSS to operate in accumulation mode, including the introduction of dedoping agents.[9,10] Additionally, the development of other

P. Y. Ho, O. Ditzer, H. Zhang, R. Thümmler, M. Al-Hussein, N. Sun, F. S.-C. Lissel
Leibniz Institute for Polymer Research (IPF) Dresden
Hohe Str. 6, 01069 Dresden, Germany
E-mail: sun@ipfdd.de; franziska.lissel@tuhh.de, lissel@ipfdd.de
P. Y. Ho, H. Zhang, F. S.-C. Lissel
Hamburg University of Technology (TUHH)
Denickestr. 17, 21073 Hamburg, Germany

The ORCID identification number(s) for the author(s) of this article can be found under https://doi.org/10.1002/adfm.202412559

DOI: 10.1002/adfm.202412559

O. Ditzer, R. Thümmler
Faculty of Chemistry and Food Chemistry
Technische Universität Dresden
01062 Dresden, Germany
A. Solgi, H. Kleemann
Dresden Integrated Center for Applied Physics and Photonic Materials (IAPP) and Institute for Applied Physics
Technische Universität Dresden
Nöthnitzer Str. 61, 01187 Dresden, Germany
M. Al-Hussein
Physics Department
The University of Jordan
Amman 11942, Jordan
H. Kleemann
Micro- and Nanoelectronic Systems
Faculty of Electrical Engineering and Information Technology TU Ilmenau
Gustav-Kirchhoff-Str. 1, 98693 Ilmenau, Germany

OMIECs operating in accumulation mode has gained significant interest. Various synthetic strategies have been explored towards this end, including the use of ionic side chains to balance charges during operation and the synthesis of block copolymers combining semiconducting polymers with polyelectrolytes to improve ionic mobility within the materials.[11–14]

Among the various synthetic strategies, the most widely used approach involves attaching polar ethylene glycol (EG) side chains to monomers commonly used to obtain high-performance semiconducting polymers (SCPs). The modification with EG side chains allows good electron transport and at the same time imparts hydrophilicity to the polymers, leading to a significantly enhanced ionic interaction.

This strategy has been successfully used to develop state-of-the-art OMIECs (e.g., p(g2T2-g4T2), μC^* = 522 F cm^{-1} V^{-1} s^{-1}, transconductance (g_m) = 6.5 mS).[15] However, the approach requires complicated synthetic steps and often results in monomers that are difficult to be purified, ultimately leading to a low overall yield.[16–18] Also, the EG side chains in the hydrophilic channel material tend to swell upon contact with the electrolyte, weakening interaction between crystalline regions, and hindering efficient electron transport along the channel.[19] Most high-performance SCPs feature alkylated side chains, rendering them hydrophobic. While hydrophobicity reduces swelling[20] and may lead to smaller changes in microstructure, these materials are generally unsuitable for physiological environment since they do not interact efficiently with an aqueous medium. Nonetheless, considering their established synthetic routes and commercial availability, developing methods to enable the utilization of conventional SCPs in OECTs would represent a significant advancement. To achieve this, different post-modification methods were explored. For example, Huang et al. demonstrated that using porous materials (both hydrophobic and hydrophilic) in OECTs leads to an improved set of parameters including transconductance, g_m, and μC^*.[21] However, achieving consistent performance is challenging due to the poor reproducibility of porosity.

Another approach involves introducing an interlayer, typically composed of an ionic liquid (e.g., 1-ethyl-3-methylimidazolium-bis(trifluoromethylsulfonyl)imide, [EMIM][TFSI]) and a gel matrix (e.g., poly(vinyliden fluoride-co-hexafluorpropylene), PVDF-HFP)) between the hydrophobic channel and aqueous electrolyte.[22,23] During operation, ion exchange within this interlayer injects [TFSI] anions into the channel, enabling efficient volumetric doping and thereby enhancing OECT performance. However, ionic liquids are highly miscible with polar solvents such as water. This affects not only the device performance, but also can lead to a release of potentially harmful substances when used in physiological environments.

Here, we present a new strategy to enable the utilization of hydrophobic SCPs in OECTs by incorporating PEGylated gold nanoparticles (AuNPs) into the polymers. We envision that the incorporation of AuNPs can significantly improve μC^* by enhancing both key parameters:

i. Increasing electronic charge carrier mobility: AuNPs have been shown to enhance charge carrier mobility of composites,[24,25] making them promising fillers to boost μ; and

ii. Enabling ionic transport: AuNPs offer remarkable flexibility for surface modification.[26,27] Looking at the existing OMIECs, tethering polar poly(ethylene glycol) (PEG) side chains is so far the most effective and most widely used strategy, as it can greatly enhance a material's ionic conductivity. This approach, while synthetically challenging for conjugated polymers, is easily implemented for AuNP using, e.g., ligand exchange. The AuNPs with PEG shell can then enable ionic transport by providing hydrophilic sites in the hydrophobic polymer matrix, facilitating efficient ion penetration into the channel. Also, the particulate filler is expected to perturb the polymer chain packing, leaving spaces and channels for ion penetration to further strengthen its ionic interaction. Finally, for polymer thin films with thicknesses below the diameter of the nanoparticles, the AuNPs could be partly exposed to the electrolyte, leading to hydrophilic spots on the channel surface, which might act as interlayer, and uniformly sized and distributed PEG/SCP interfaces could enable efficient ion transportation and enhanced electrolytic ion channel interaction.

Therefore, in this study, PEGylated AuNP is synthesized and mixed with commercially available poly(3-hexyl-thiophene) (P3HT) and poly(2,5-(2-octyldodecyl)-3,6-diketopyrrolopyrrole-alt-5,5-(2,5-di(thien-2-yl)thieno[3,2-b]thiophene) (PDPP-TT). Subsequently, OECT devices with films containing different AuNP weight ratios are fabricated and the critical performance parameters such as transconductance (g_m) and μC^* are evaluated. Electrical impedance spectroscopy (EIS), spectro-electrochemical (SEC) analysis and grazing-incidence wide-angle X-ray scattering (GIWAXS) measurement are employed to understand the role of AuNP in enhancing ionic and electrical performance.

2. Results and Discussion

In our study, we integrated AuNPs with hydrophilic PEG shells as nanoparticulate fillers into high-performance hydrophobic SCPs (**Figure 1**).

Citrate stabilized AuNPs with a size of 45 nm were synthesized using a step-growth method,[28] followed by a ligand exchange with thiol-PEG to afford the PEGylated AuNPs. After the ligand exchange, the AuNPs were transferred to chloroform, which can be readily used to blend with hydrophobic polymers. Two commercially available SCPs (i.e., P3HT and PDPP-TT) with thoroughly studied electrical properties were selected as polymer matrix. Prior to use, the SCPs were purified by Soxhlet extraction (details on the purification procedure are given the experimental section). Transmission electron microscopy (TEM) images (**Figure 2a**) show a 2 nm PEG shell on the AuNPs. This shell likely serves as a hydrophilic interfacial layer between the hydrophobic SCP and AuNP, enabling the formation of an ion-permeable interface between P3HT and AuNP as indicated by the reduced contact angle upon mixing the AuNP (Figure S1 and Table S1, Supporting Information). Also, from the TEM and AFM images, we observed that the PEGylated AuNPs are evenly distributed in the P3HT matrix with no significant aggregation (Figure 2b).

Composite systems with different AuNP weight ratios (0, 5, 10, and 20 wt%) were fabricated to implement our proposed strategy. To confirm the stability of AuNPs in the P3HT matrix

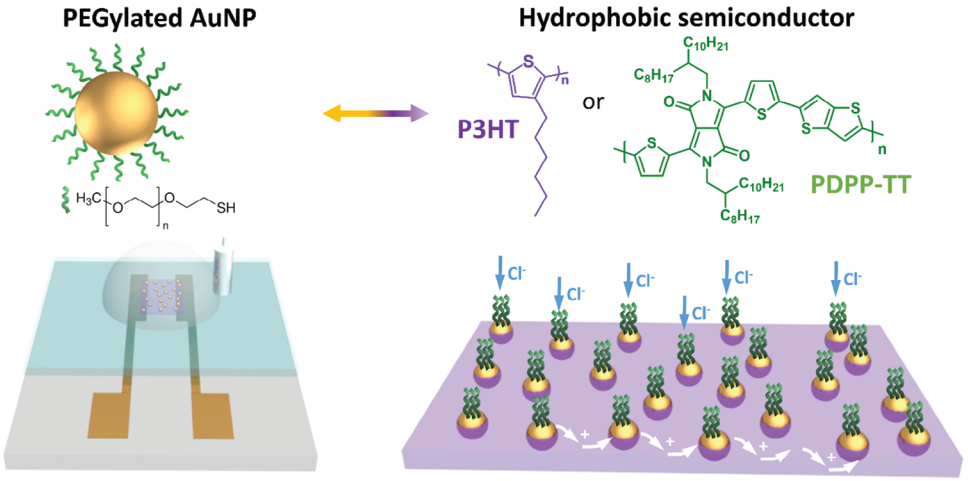

Figure 1. Schematic illustration of mixing PEGylated AuNP into high-performance hydrophobic SCPs to boost ionic and electronic transportation in the channel.

during operation and evaluate their potential as an interlayer between the channel and the electrolyte, AFM images of pristine 5 wt% AuNP/P3HT film and 5 wt% AuNP/P3HT film after ten cycles of 4 s potential pulses (2 s at -0.8 V followed by 2 s at 0 V, vs Ag/AgCl) were compared (Figure 2c,d). Following the cycling experiments, the sample was soaked in Millipore water for 30 minutes and then thoroughly rinsed with fresh Millipore water. No loss of AuNPs is detected, indicating a robust embodiment of the particulate filler into the P3HT channel matrix. For further clarification, the same procedure was performed on the 50 wt% AuNP/ P3HT (Figure S2, Supporting Information). At the same time, the presence of a porous structure, which could also

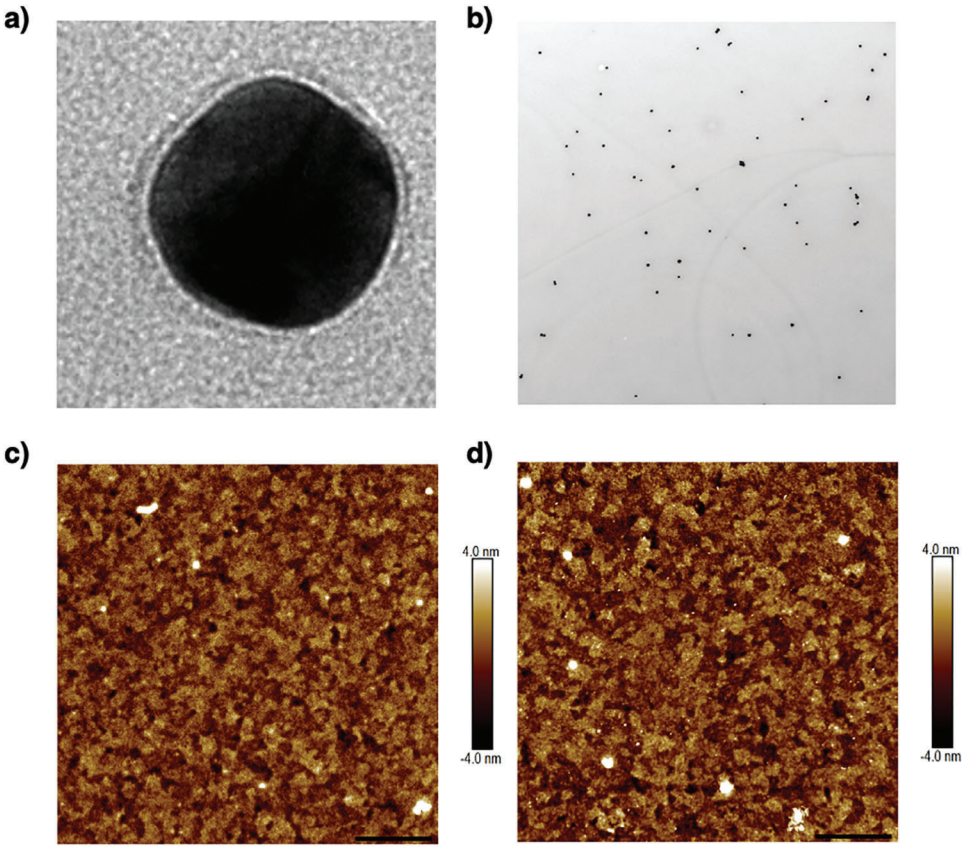

Figure 2. a) A zoomed-in image of a AuNP (diameter ≈ 45 nm, shell thickness ≈ 2 nm) and b) TEM image of drop-casted 5 wt% AuNP/P3HT film. c) Pristine 5 wt% AuNP/P3HT and d) 5 wt% AuNP/P3HT after 10 gate pulses (amplitude = −0.8 V, frequency = 0.25 Hz, duty cycle = 50%).

contribute to the improvement of OECT performance,[21] is excluded, confirming that the enhancement in OECT performance stems from the composites rather than the formation of a porous structure. The results suggest that the pegylated AuNPs serve as an interlayer between the SCP channel and the electrolyte.

To optimize the electrical performance and ionic interaction of the OECT channel, composite films with varying AuNP/P3HT weight ratios were used as the channel materials. Various electrical characterizations (i.e., transfer and output characterizations, operational stability) were carried out, and relevant device and material performance parameters (e.g., transconductance (g_m), μC^* and turn-on time) were determined. Transfer curves of OECT devices using pure P3HT, 5 wt% AuNP in P3HT (i.e., 5 wt% AuNP/P3HT), 10 wt% AuNP in P3HT (i.e., 10 wt% AuNP/P3HT) and 20 wt% AuNP in P3HT (i.e., 20 wt% AuNP/P3HT) were measured within a gate potential range of 0.2 to -0.8 V versus Ag/AgCl. A 0.1 M NaCl(aq) solution was used as the electrolyte and -0.6 V was applied across the source-drain channel, so that the channel operates in saturation regime (please see Figure S3, Supporting Information, for the output curves). Equation 1 was used to estimate the transconductance g_m:[29]

$$g_m = (Wd/L)\,\mu C^* \left(V_{th} - V_g\right) \quad (1)$$

where W, d, and L are channel width, thickness and length, respectively. μ represents the hole carrier mobility, C^* the volumetric capacitance, V_{th} the threshold voltage, and V_g the gate voltage.

For all composites, the V_{th} as well as maximum g_m values were obtained from 10 to 16 devices. In case of the 5 wt% AuNP/P3HT composite, an increase in on-current is observed compared with OECTs fabricated with pure P3HT (**Figure 3**a–d), while only a slight decrease in V_{th} was noted (Figure S4, Supporting Information). This indicates that the influence of the AuNP filler on the HOMO energy level of P3HT is negligible.[10] Additionally, a significant increase in both transconductance and on-off ratio of 5 wt% AuNP/P3HT OECTs compared to pure P3HT was observed (i.e., from 0.3 mS for pure P3HT to >0.7 mS for 5 wt% AuNP/P3HT). For a better comparison, the g_m values are normalized by the channel volume (i.e., $g_{m,n}$). As illustrated in Figure S5 (Supporting Information), the $g_{m,n}$ peaks for 5 wt% AuNP/P3HT OECT, demonstrating a 2 to 3-fold increase compared to that of pure P3HT OECT (from 7 to 17 S cm^{-1}). This indicates a significant enhancement in the ion/electron transport properties of the 5 wt% composite thin film. Meanwhile, increasing the AuNP weight ratios further to 10 wt% and 20 wt% does not improve transconductance (8.5 and 5 S cm^{-1}, respectively).

μC^* values were extracted from the slopes of g_m versus $Wd/L(V_{th} - V_g)$ plots (Figure 3e). μC^* increased from 38 F cm^{-1} V^{-1} s^{-1} (pure P3HT) to 98 F cm^{-1} V^{-1} s^{-1} (5 wt% AuNP/P3HT), followed by a slight decrease to 74 F cm^{-1} V^{-1} s^{-1} (both 10 wt% and 20 wt% AuNP/P3HT). To determine whether this increase of μC^* in the presence of 5 wt% AuNP can be attributed to an increase of charge carrier mobility (μ) or volumetric capacitance (C^*), electrochemical impedance spectroscopy (EIS) measurements were performed. This technique allows to elucidate the change of the ionic interaction of P3HT upon mixing AuNP. The capacitance evaluation was done by fitting Randles circuit in impedance measurements (Figures S6 and S7, Supporting Information). As shown in Figure 3f, the C^* values experienced an increase from 74.59 F cm^{-3} for pure P3HT to 87.20 F cm^{-3} for 5 wt% AuNP/P3HT (the thickness of channel is estimated by AFM measurements as shown in Table S2, Supporting Information). Further increasing the AuNP weight ratio in the composite films resulted in higher C^* values compared to pure P3HT film (i.e., 92.17 F cm^{-3} and 87.58 F cm^{-3} for 10 wt% and 20 wt% AuNP/P3HT films, respectively), indicating that the AuNP filler indeed contributes to the ionic interaction between the channel material and electrolyte, allowing for the generation of more charges in the composite thin films compared to pure P3HT.

The hole charge carrier mobilities were calculated using the Bernards and Malliaras model for steady-state OECT behavior[30] (as shown in **Table 1** and Equation S1, Supporting Information), and all the values are of the same order of magnitude as the non-thermally annealed P3HT.[31] Overall, a significant increase in hole charge carrier mobility was observed for the 5 wt% AuNP/P3HT composite OECT (i.e., 9.69 × 10^{-3} vs 5.35 × 10^{-3} cm^2 V^{-1} s^{-1} for pure P3HT OECT), demonstrating the role of AuNP in enhancing both the channel/ion interaction and the electron transport in the channel. With higher AuNP loadings (i.e., 10 wt% and 20 wt%), a decrease in mobility was observed. Although shrinkage of both lamellae and π–π distances in P3HT domain was still observed in 10 wt% and 20 wt% AuNP/P3HT thin films (as shown later in the GIWAXS measurements section), which is beneficial to electronic transport,[32] the larger amount of AuNP in these thin films could presumably increase the probability of charge trapping,[33] leading to the observed decrease in mobility values.

The operational stability of OECTs with different composites was investigated. Devices were switched between their on-state (V_g = -0.8 V) and off-state (V_g = 0.2 V) for 22 s each, and the change in I_d over 40 cycles was recorded. **Figure 4**a shows that a pure P3HT channel required around 30 cycles until the on-state I_d reaches a plateau. In contrast, the 5 wt% AuNP/P3HT channel exhibited consistent on/off switching throughout all 40 cycles (Figure 4b), indicating more efficient ion transport in the 5 wt% AuNP/P3HT channel compared to the pure P3HT channel. This enhanced performance is likely due to the hydrophilic PEG interlayer provided by the AuNPs, enabling faster and more complete doping. In pure P3HT, ion penetration through the hydrophobic channel may be slower, necessitating more cycles to reach a similar level of doping. OECT devices with 10 wt% and 20 wt% AuNP/P3HT composite channels were also studied (Figure S8, Supporting Information), with both showing more stable cyclic performance than the pure P3HT device, highlighting the improved operational stability achieved by incorporating AuNPs. By fitting the data to an exponential decay function, the turn-on time (τ_{on}) and the turn-off time (τ_{off}) for both P3HT and composite devices were extracted (Figure S9, Supporting Information). The composite OECT devices exhibited significantly shorter τ_{on} and τ_{off} values (4.5–5.6 s and 1.1–1.8 s, respectively) compared to the pure P3HT device (15.5 and 2.3 s, respectively), further demonstrating the ability of AuNPs to enhance ion transport in the channel.

To evaluate the broader applicability of our strategy to other polymer systems, OECT devices with pure PDPP-TT and 2 wt% AuNP/PDPP-TT channels were fabricated, and $g_{m,n}$ and μC^* were measured. The incorporation of AuNP resulted in a significant increase in $g_{m,n}$ from 9.09 to 22.68 S cm^{-1} (Figure S10,

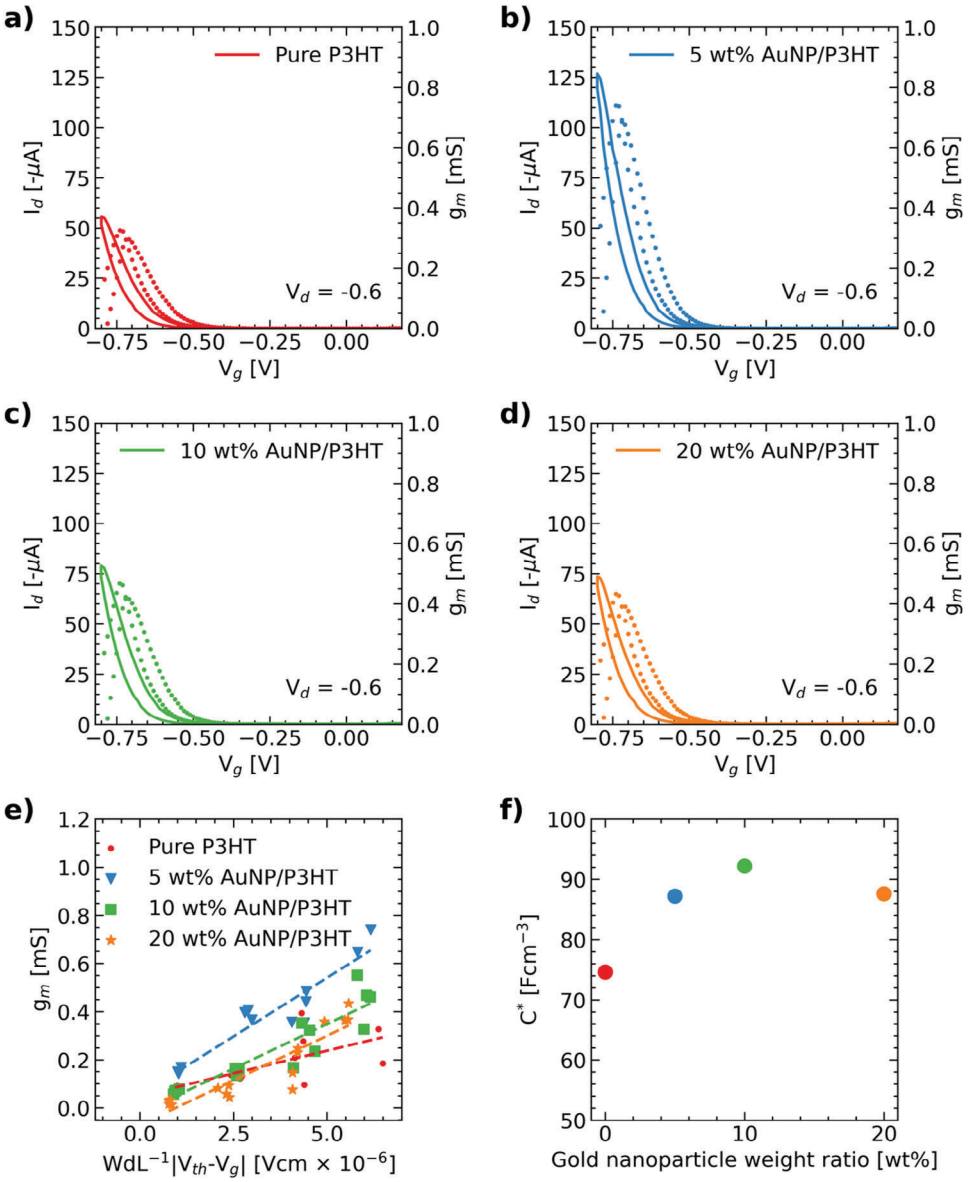

Figure 3. a–d) Transfer characteristic of different composites (solid lines = drain current (I_d), dotted lines = g_m. Condition: 0.1 M NaCl electrolyte, scan rate = 0.24 V s^{-1}). e) g_m versus W dL^{-1}(V_{th} - V_g) plot of different composite films for the extraction of material parameter μC^*. f) volumetric capacitance, C^*, of different composite films.

Table 1. OECT parameters of different AuNP/P3HT composites.

AuNP weight ratio [wt%]	On-off ratio	V_{th} [V]	τ_{on} [s]	τ_{off} [s]	$g_{m,n}$ [S cm^{-1}]	C^* [F cm^{-3}]	μC^* [F cm^{-1} V^{-1} s^{-1}]	μ [× 10^{-3} cm^2 V^{-1} s^{-1}]
0	800	−0.62	15.46 ± 0.81	2.31 ± 0.07	6.97	74.59	37.57 ± 10.87	5.35 ± 1.95
5	1600	−0.61	4.50 ± 0.11	1.81 ± 0.07	17.15	87.20	97.55 ± 10.21	9.69 ± 2.02
10	1100	−0.62	5.56 ± 0.25	1.35 ± 0.09	8.27	92.17	74.02 ± 8.55	4.80 ± 1.04
20	1400	−0.62	4.49 ± 0.17	1.13 ± 0.06	4.81	87.58	74.07 ± 9.04	3.12 ± 1.69

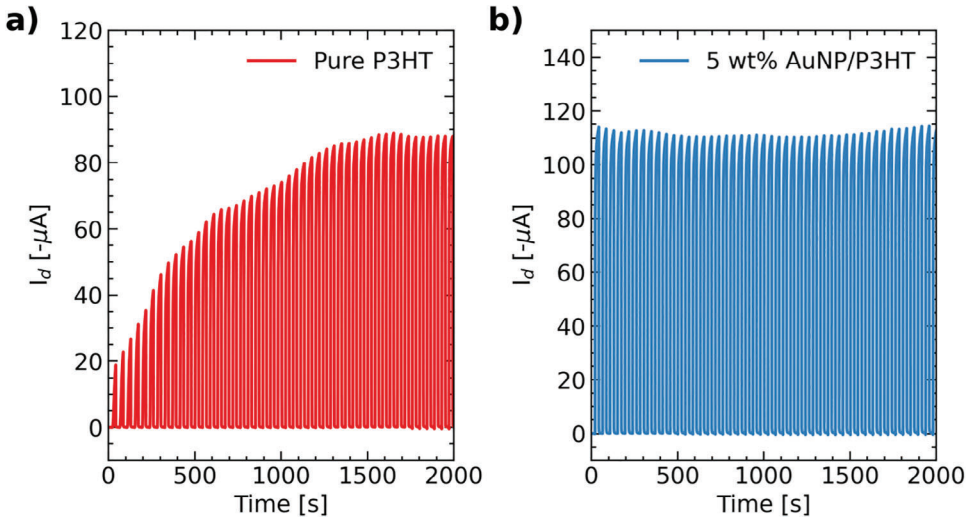

Figure 4. Operational stability characterization of OECTs with a) pure P3HT and b) 5 wt% AuNP/P3HT channels. The devices are switched on with V_g = -0.8 V (duration = 22 s) and switched off with V_g = 0.2 V (22 s) (condition: 0.1 M NaCl as electrolyte).

Supporting Information), demonstrating that the composite formation approach can be effectively extended to different SCPs. Additionally, the μC^* values increase from 42.90 F cm^{-1} V^{-1} s^{-1} (pure PDPP-TT) to 173.81 F cm^{-1} V^{-1} s^{-1} (2 wt% AuNP/PDPP-TT) (Figure S11, Supporting Information).

To understand the influence of AuNPs on the electrochemical doping of P3HT during operation, spectro-electrochemical (SEC) analysis of pure P3HT and 5 wt% AuNP/P3HT thin films was carried out. The UV-vis absorption spectra of the composite thin films with different AuNP/P3HT weight ratios were recorded. No significant changes in absorption pattern and intensity were observed from pure P3HT to 10 wt% AuNP/P3HT thin films (Figure S12, Supporting Information). However, when a gate potential was applied to pure P3HT and the 5 wt% AuNP/P3HT film in the presence of a 0.1 M NaCl electrolyte solution, a significant difference was observed (**Figure 5**): For pure P3HT, the absorption intensity at 520 nm (i.e., π–π^*) decreased from 1 to 0.7 upon application of 0.8 V versus Ag/AgCl to the ITO working electrode. Concurrently, the absorption intensity at approximately 800 nm (i.e., polaron absorption) increased from 0.15 to 0.36. These changes indicate the occurrence of P3HT oxidation.[34,35] When the same potential is applied to the 5 wt% AuNP/P3HT film on an ITO electrode, the π–π^* absorption intensity decreases from 1 to 0.55, while the polaron absorption intensity increases from 0.05 to 0.41. At 0.8 V, the absorbance ratio of the π–π^* transition to polaron absorption in the 5 wt% AuNP/P3HT film (0.55 and 0.41, respectively) is significantly smaller than that of the pure P3HT film (0.7 and 0.36, respectively). The significantly higher proportion of polarons generated in the composite thin film under gate potential suggests that the P3HT domain in the presence of 5 wt% AuNP undergoes more thorough oxidation compared to pure P3HT under identical bias conditions. This observation supports the conclusion that AuNPs enhance the efficiency of volumetric doping in P3HT, consistent with the previously noted increase in C^* values and faster response speed for the composite thin films.

While an enhancement of ionic performance in all composite OECTs is demonstrated by electrical impedance measurements,

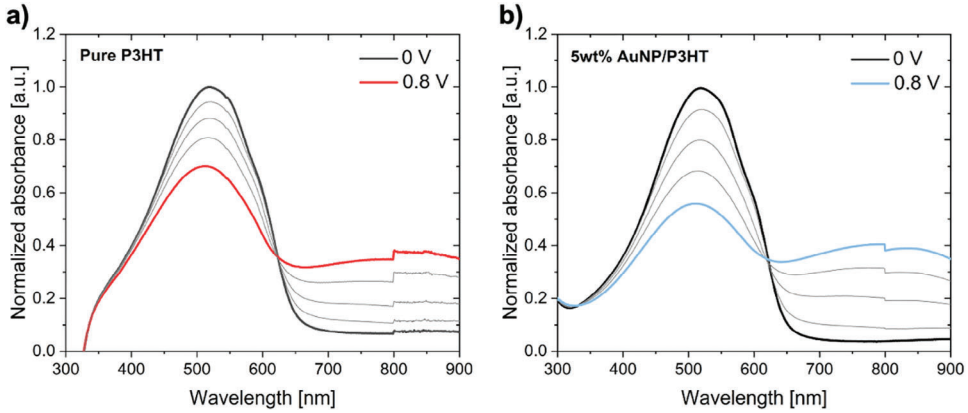

Figure 5. Spectro-electrochemical analysis of a) pure P3HT and b) 5 wt% AuNP/P3HT thin films. Condition: working electrode = ITO; counter electrode = platinum wire; reference electrode = Ag/AgCl pallet; electrolyte = 0.1 M $NaCl_{(aq)}$.

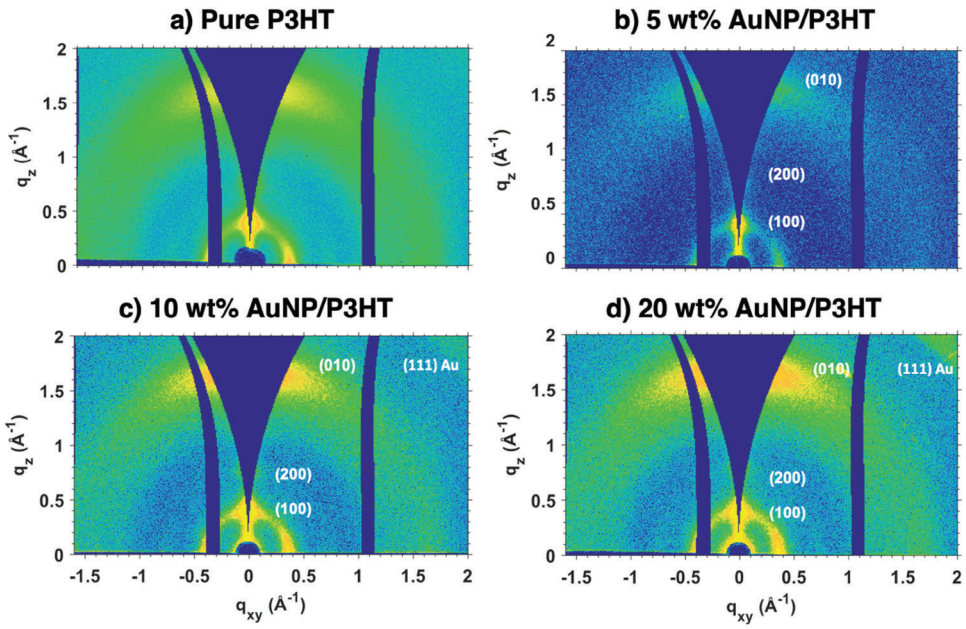

Figure 6. GIWAXS reflection patterns of a) pure P3HT, b) 5 wt% AuNP/P3HT, c) 10 wt% AuNP/P3HT and d) 20 wt% AuNP/P3HT.

response time characterizations, and SEC analysis, the reason for the enhanced electrical performance of the composite thin films remains ambiguous. Therefore, grazing-incidence wide-angle X-ray scattering (GIWAXS) measurements were performed. The 2D GIWAXS patterns of pure P3HT, 5 wt% AuNP/P3HT, 10 wt% AuNP/P3HT and 20 wt% AuNP/P3HT are shown in **Figure 6**. For pure P3HT, 10 wt% AuNP/P3HT and 20 wt% AuNP/P3HT thin films, the (100) and (200) lamellar stacking reflections of P3HT crystallites could be seen in both in-plane and out-of-plane directions relative to the substrate, while the (010) π–π stacking reflection appeared mainly in the out-of-plane direction. This indicates that the P3HT crystallites in these samples predominantly adopt a face-on orientation. To assess the orientation of the P3HT lamellae relative to the substrate, tube cut of the (010) reflection with an azimuthal range χ (0° to -90°) were extracted from the 2D GIWAXS patterns of all films, as shown in Figure S13 (Supporting Information). The (010) π–π stacking reflection of the 5 wt% AuNP/P3HT thin film appeared more isotropic, indicating a more random orientation of the P3HT crystallites in this sample. This less preferential orientation of P3HT crystallites likely enhances ion interactions within the channel material,[36] which may account for the highest C^* value observed in the 5 wt% AuNP/P3HT thin film among all composite films. Additionally, the (111) reflection was detected at AuNP contents above 10 wt% (Figure S14, Supporting Information). To further elucidate the distribution of AuNPs within the P3HT matrix, we performed AFM measurements. As shown in Figure S15 (Supporting Information), the 5 wt% AuNP/P3HT thin film exhibited a minimal amount of AuNP islands, whereas more pronounced island formation was observed at 10 wt% and 20 wt% AuNP loadings. This might explain the small decrease in C^* values from 10 wt% to 20 wt% AuNP/P3HT composite films as the reduced AuNP/P3HT interfacial area diminishes ion transport efficiency. Moreover, all AuNP composite films exhibited smaller π–π (3.77 to 3.79 Å) and lamellar (16.61 to 16.69 Å) distances compared to the pure P3HT thin film (3.88 Å and 17.26 Å respectively). Therefore, at the optimal AuNP ratio (5 wt%), this could contribute to the increase in hole carrier mobility[37] and thus the μC^* values in all composite films at different AuNP ratios. While the exact mechanism behind the reduction in π–π stacking and lamellar distances remains unclear, we hypothesize that this crystallite contraction may be driven by interfacial stress. This stress could arise at the interface between the hydrophilic AuNPs and the hydrophobic P3HT domains, likely due to differences in surface tension, as indicated by our contact angle measurements.[38,39] This interfacial stress might play a key role in altering the structural arrangement within the composite film.

3. Conclusion

This study demonstrates integrating gold nanoparticles (AuNPs) with semiconducting polymers (SCPs) as a simple and effective strategy to enhance both the ionic and electrical properties of hydrophobic channels in organic electrochemical transistors (OECTs). The incorporation of AuNPs in both P3HT and PDPP-TT channels results in significant OECT performance improvements. Comprehensive characterizations of the AuNP/P3HT composites—including contact angle measurements, GIWAXS, electrical impedance spectroscopy, response time analyses, and SEC evaluations—demonstrate that the incorporated AuNPs not only provide hydrophilicity to the composite channels, but also modify the thin film morphology based on their concentration, allowing for more efficient ion transport and more thorough doping of P3HT domain. In all composite films, the incorporation of AuNPs also causes a contraction of the P3HT crystalline domains. At the optimal AuNP/P3HT ratio (5 wt%), the film exhibits the shortest π–π stacking and lamellar distances, which contributes to improved hole mobility. These combined effects result in a substantial enhancement in transconductance and μC^*, leading to significantly improved device performance.

Consequently, this work expands the range of accessible semiconducting materials for OECT applications without necessitating complex synthetic modifications, simplifying the search for new OECT materials. Ongoing research in our lab aims to further functionalize AuNPs to optimize ion and electron transport in OECTs.

4. Experimental Section

Materials: Regioregular P3HT was purchased from Sigma Aldrich and used after Soxhlet purification with methanol, acetone, and extraction with chloroform, followed by. All other chemicals and solvents were used without further purification after purchase unless stated otherwise.[6]

Synthesis: PEGylated-AuNP citrate stabilized AuNPs were first synthesized by a step-growth method. Before the start of the synthesis, all glassware and stir bars were cleaned with aqua regia and rinsed three times with Millipore water. The procedure began with the preparation of seeds. First, 150 mL of 2.2×10^{-3} M sodium citrate solution was heated to boiling (100 °C) in a 1 L conical flask under stirring. 1 mL of 25×10^{-3} M $HAuCl_4$ was quickly added. After 10 min, the solution changed to a pink color, indicating seed formation. The solution was cooled to 90 °C, and 1 mL of 25×10^{-3} M $HAuCl_4$ was added. After stirring for 30 min at 90 °C, another 1 mL of 25×10^{-3} M HAuCl4 was added and stirred for 30 min. 82.8 mL of Millipore water and 3.12 mL of 60×10^{-3} M sodium citrate solution were added to the flask. The temperature was maintained at 90 °C, and 1.56 mL of 25×10^{-3} M $HAuCl_4$ was added and stirred for 30 min. Then, another 1.56 mL of the $HAuCl_4$ solution was added and stirred at 90 °C for 30 min. For Step 3, 130.9 mL of Millipore water and 4.94 mL of 60×10^{-3} M sodium citrate solution were added, and the solution was kept at 90 °C. Then, 2.47 mL of 25×10^{-3} M $HAuCl_4$ was added and stirred for 30 min, and this operation was repeated once. In Step 4, 207 mL of Millipore water and 7.8 mL of 60×10^{-3} M sodium citrate solution were added to the flask, and the solution was maintained at 90 °C, followed by the addition of 3.9 mL of 25×10^{-3} M $HAuCl_4$. After stirring for 30 min, another 3.9 mL of 25×10^{-3} M $HAuCl_4$ was added, and the solution was stirred for an additional 30 min. Finally, in Step 5, 327.4 mL of Millipore water and 12.36 mL of 60×10^{-3} M sodium citrate solution were added. The solution was kept at 90 °C, and 6.18 mL of 25×10^{-3} M $HAuCl_4$ was added and stirred for 30 min. Another 6.18 mL of 25×10^{-3} M $HAuCl_4$ was then added, and the solution was stirred for another 30 min, resulting in a final volume of 957.53 mL and around 50 nm gold nanoparticles. After obtaining the desired size of citrate-AuNPs, a ligand exchange was carried out by using thiol-PEG (6 kDa). 1 mL of chloroform with 10 mg mL^{-1} thiol-PEG was added to 10 mL of aqueous AuNP solution (2.0 mg mL^{-1} Au), followed by vented for 2 min. After adding 5 mL of methanol and another 1 mL chloroform, the mixture was shaken and vented again for 2 min. Subsequent shaking overnight secured the complete ligand exchange. Then the PEGylated-AuNPs in chloroform phase were purified by three centrifugation–redispersion cycles (500 rcf for 1 h, redispersion in chloroform).

Atomic Force Microscopy: Polymer solutions with different weight ratios of AuNP were spin-coated on hexamethyldisilizane (HMDS)-treated silicon substrates at 2000 rpm for 120 s. The substrates were treated by air-plasma, followed by immediate transfer into a petri dish with 200 µL of HMDS. After 15 min, the substrates were heated at 100 °C for another 15 min. The surface morphology of the films was examined using ScanAsyst mode on a Bruker FastScan AFM equipped with a ScanAsyst Air Probe. Nanoscope analysis 2.0 software was used for analysis. To determine the thickness of the films, areas of the samples were removed by scratching, and the step height of the scratches was measured at three different locations on the film and averaged

OECT Fabrication: Quartz-coated glass substrates were sonicated in acetone and isopropanol for 10 min each. After that, source-drain electrodes (i.e., Ti = 5 nm, Au = 30 nm) were defined by E-beam evaporation through a shadow mask. Photolithography was performed with the use of SU-8 2002 so that only the contact pads of the source/drain electrodes and a defined area at the channel were exposed. The photolithography procedure and parameters are adopted from the data sheet provided by the company. Finally, 50 µL of 5 mg mL− composite solutions were spin-coated on the patterned substrates at 2000 rpm for 120 s and the devices were physically separated from each other by scratching.

OECT Characterization: Transfer, output and operational stability characterizations were evaluated under ambient condition on a probe station (MPI) connected to a Keithley 2612b SMU (Keithley Instruments, USA). An Ag/AgCl pallet with silver wire (Science Products GmbH) was used as the gate electrode. 0.1 M $NaCl_{(aq)}$ was used as the supporting electrolyte. The SMU was controlled by the SweepMe! software (sweepme.net). For all transfer measurements, the source–drain voltage was maintained at −0.6 V and each gate voltage step was set to 0.01 V with a software delay time of 0.1 s. The range of gate voltage applied was between 0.2 and −0.8 V for the P3HT-based composite OECTs and between 0.1 and −1 V for the PDPP-TT-based composite OECTs. For all output measurements, drain voltage step was set to 0.002 V with a software delay time of 0.1 s. The range of applied drain voltage was between 0.5 and −0.5 V while the gate voltage was constant. For all operational stability measurements, V_g was alternating between -0.8 V and 0.2 (22 s each) in order to achieve on and off states, respectively. A constant V_d (i.e., -0.4 V) was applied to the channel.

Electrical Impedance Measurement: Impedance measurements were conducted using a Metrohm Autolab PGSTAT302N (Filderstadt, Germany) in the potentiostatic mode. The measurements were performed with an RMS amplitude of 25 mV and DC offset of 0.8 V. The scan range for the measurements spanned from 10^5 to 10^{-1} Hz.

SEC Analysis: ITO-coated glass substrates were cleaned by sonicating in acetone and isopropanol for 10 min each. After that, the 5 mg mL^{-1} pure P3HT and 5 wt% AuNP/P3HT solutions were diluted 50 times and drop-casted onto the ITO substrates. The as-cast films were dried under vacuum for 1 h. 0.1 M NaCl(aq) solution was used as the supporting electrolyte. The SEC characterization was carried out with Metrohm Autolab PGSTAT204. The working electrode was connected to the ITO substrates with polymer thin film. The counter was connected to a platinum wire. The reference electrode was connected to a Ag/AgCl pallet via silver wire. UV–vis–NIR spectra of the devices after the application of different potentials were recorded on Cary 7000.

GIWAXS Measurement: Silicon substrates were sonicated in acetone and isopropanol for 10 min each. After that, the substrates were treated with plasma, followed by immediate transfer into a petri dish with 200 µL of HMDS. After 15 min, the substrates were heated at around 100 °C for another 15 min. 50 µL of 5 mg mL^{-1} P3HT, 5 wt% AuNP/P3HT, 10 wt% AuNP/P3HT and 20 wt% thin films were prepared by spin-coating at 2000 rpm for 120 s. The as-cast thin film samples were used for the measurements without thermal annealing. GIWAXS experiments were performed using GANESHA 300XL+ system (SAXSLAB ApS, Lyngby/Denmark). The instrument is equipped with a Pilatus 300K detector, Cu X-ray source operated at 50 kV/0.6 mA ($\lambda = 1.5408$ Å), and a three-slit collimation system. An incident angle of 0.2° and a sample-to-detector distance of 102.2 mm were used. The data were analyzed using GIXSGUI program. The radially integrated line profiles of the GIWAXS patterns were fitted using individual Gaussian functions. The lamellar spacing and coherence length were then calculated from the (100) peak position, q100, and full width at half maximum, Δq100, according to the following equations: $2\pi/(q100)$ and $2\pi/(\Delta q100)$, respectively. For in-plane and out-of-plane line cuts, the intensity was averaged over an azimuthal range of 0°−17°, and 71°−88°, respectively.

Contact Angle Measurement: The thin film samples were spin-coated on HMDS-treated quartz-coated glass substrates with the aforementioned spin-coating parameters. Contact angle measurement was performed on an OCA 40 Micro Automatic Contact Angle Meter and analyzed with SCA 20 (DataPhysics Instruments GmbH, Filderstadt, Germany). The device was equipped with a 7-fold zoom lens with integrated fine focus (± 4 mm), a microscopic lens (20-fold with 7.5 to 55 magnifications; field of view with 1/2 in. standard camera 0.85 × 0.64 to 0.116 × 0.087 mm) and an image processing system (CCD camera with a resolution of 768 × 576 pixels,

frame grabber compatible with Euronorm CCIR, 60 images per second). Every 13th frame was used for analysis. Milli-Q grade water was used. Dynamic contact angle measurements were performed by first predispensing a volume of 5 µL of water droplet, followed by dispensing another 5 µL (0.25 µL s^{-1}) and withdrawing 5 µL (0.25 µL s^{-1}). Frames used for calculations were selected according to the droplet movement periods. Advancing and receding contact angle were calculated using averages ranges of leaning tangents.

Supporting Information

Supporting Information is available from the Wiley Online Library or from the author.

Acknowledgements

This work has received funding from the European Innovation Council (EIC) under the project ESiM (grant agreement No. 101046364). F. S.-C. L. thanks the AGYA project of the Berlin-Brandenburg Academy of Sciences and Humanities (BBAW). Financial support of the Ingeborg-Gross Stiftung is gratefully acknowledged. M.A.H. thanks the University of Jordan and Leibniz-Institute for Polymer Research Dresden (IPF Dresden) for financial support. H. Z. and R. T. acknowledge support from DFG within GRK 2767: Supracolloidal Structures: From Materials to Optical and Electronic Devices, Project number 451785257.

Open access funding enabled and organized by Projekt DEAL.

Conflict of Interest

The authors declare no conflict of interest.

Data Availability Statement

The data that support the findings of this study are available from the corresponding author upon reasonable request.

Keywords

gold nanoparticles, hydrophobic semiconductors, organic electrochemical transistors (OECT)

Received: July 15, 2024
Revised: October 28, 2024
Published online:

[1] D. Khodagholy, T. Doublet, P. Quilichini, M. Gurfinkel, P. Leleux, A. Ghestem, E. Ismailova, T. Hervé, S. Sanaur, C. Bernard, G. G. Malliaras, *Nat. Commun.* **2013**, *4*, 1575.
[2] P. Leleux, J. Rivnay, T. Lonjaret, J. Badier, C. Bénar, T. Hervé, P. Chauvel, G. G. Malliaras, *Adv. Healthcare Mater.* **2015**, *4*, 142.
[3] P. Gkoupidenis, N. Schaefer, B. Garlan, G. G. Malliaras, *Adv. Mater.* **2015**, *27*, 7176.
[4] Y. van de Burgt, E. Lubberman, E. J. Fuller, S. T. Keene, G. C. Faria, S. Agarwal, M. J. Marinella, A. Alec Talin, A. Salleo, *Nat. Mater.* **2017**, *16*, 414.
[5] Y. van de Burgt, A. Melianas, S. T. Keene, G. Malliaras, A. Salleo, *Nat. Electron.* **2018**, *1*, 386.
[6] X. Ji, B. D. Paulsen, G. K. K. Chik, R. Wu, Y. Yin, P. K. L. Chan, J. Rivnay, *Nat. Commun.* **2021**, *12*, 2480.
[7] S. Wang, X. Chen, C. Zhao, Y. Kong, B. Lin, Y. Wu, Z. Bi, Z. Xuan, T. Li, Y. Li, W. Zhang, E. Ma, Z. Wang, W. Ma, *Nat. Electron.* **2023**, *6*, 281.
[8] J. Rivnay, S. Inal, A. Salleo, R. M. Owens, M. Berggren, G. G. Malliaras, *Nat. Rev. Mater.* **2018**, *3*, 17086.
[9] M. Knoll, M. Thämer, *Electrochem. Commun.* **2011**, *13*, 597.
[10] S. T. Keene, T. P. A. van der Pol, D. Zakhidov, C. H. L. Weijtens, R. A. J. Janssen, A. Salleo, Y. van de Burgt, *Adv. Mater.* **2020**, *32*, 2000270.
[11] E. Zeglio, O. Inganäs, *Adv. Mater.* **2018**, *30*, 1800941.
[12] J. H. Kim, S. Kim, G. Kim, M. Yoon, *Macromol. Biosci.* **2020**, *20*, 2000211.
[13] B. D. Paulsen, K. Tybrandt, E. Stavrinidou, J. Rivnay, *Nat. Mater.* **2020**, *19*, 13.
[14] P. R. Paudel, J. Tropp, V. Kaphle, J. D. Azoulay, B. Lüssem, *J. Mater. Chem. C* **2021**, *9*, 9761.
[15] M. Moser, T. C. Hidalgo, J. Surgailis, J. Gladisch, S. Ghosh, R. Sheelamanthula, Q. Thiburce, A. Giovannitti, A. Salleo, N. Gasparini, A. Wadsworth, I. Zozoulenko, M. Berggren, E. Stavrinidou, S. Inal, I. McCulloch, *Adv. Mater.* **2020**, *32*, 2002748.
[16] M. Moser, A. Savva, K. Thorley, B. D. Paulsen, T. C. Hidalgo, D. Ohayon, H. Chen, A. Giovannitti, A. Marks, N. Gasparini, A. Wadsworth, J. Rivnay, S. Inal, I. McCulloch, *Angew. Chem., Int. Ed.* **2021**, *60*, 7777.
[17] H. Jia, Z. Huang, P. Li, S. Zhang, Y. Wang, J.-Y. Wang, X. Gu, T. Lei, *J. Mater. Chem. C* **2021**, *9*, 4927.
[18] G. Krauss, F. Meichsner, A. Hochgesang, J. Mohanraj, S. Salehi, P. Schmode, M. Thelakkat, *Adv. Funct. Mater.* **2021**, *31*, 2010048.
[19] L. Q. Flagg, C. G. Bischak, J. W. Onorato, R. B. Rashid, C. K. Luscombe, D. S. Ginger, *J. Am. Chem. Soc.* **2019**, *141*, 4345.
[20] N. P. Menezes, T. Nicolini, M. Barker, A. A. Mariano, C. A. Dartora, G. Wantz, N. Stingelin, M. Abbas, O. J. Dautel, D. Thuau, *J. Mater. Chem. C* **2023**, *11*, 6296.
[21] L. Huang, Z. Wang, J. Chen, B. Wang, Y. Chen, W. Huang, L. Chi, T. J. Marks, A. Facchetti, *Adv. Mater.* **2021**, *33*, 2007041.
[22] C. G. Bischak, L. Q. Flagg, D. S. Ginger, *Adv. Mater.* **2020**, *32*, 2002610.
[23] R. He, A. Lv, X. Jiang, C. Cai, Y. Wang, W. Yue, L. Huang, X. Yin, L. Chi, *Angew. Chem., Int. Ed.* **2023**, *62*, 202304549.
[24] C. Vijayakumar, B. Balan, A. Saeki, T. Tsuda, S. Kuwabata, S. Seki, *J. Phys. Chem. C* **2012**, *116*, 17343.
[25] L. Zhang, L. Wang, S. He, C. Zhu, Z. Gong, Y. Zhang, J. Wang, L. Yu, K. Gao, X. Kang, Y. Song, G. Lu, H.-D. Yu, *ACS Appl. Mater. Interfaces* **2023**, *15*, 3224.
[26] N. Sun, S. Zhang, F. Simon, A. M. Steiner, J. Schubert, Y. Du, Z. Qiao, A. Fery, F. Lissel, *Angew. Chem., Int. Ed.* **2021**, *60*, 3912.
[27] N. Sun, S. Singh, H. Zhang, I. Hermes, Z. Zhou, H. Schlicke, Y. Vaynzof, F. Lissel, A. Fery, *Adv. Sci.* **2024**, *11*, 2400752.
[28] N. G. Bastús, J. Comenge, V. Puntes, *Langmuir* **2011**, *27*, 11098.
[29] J. Rivnay, P. Leleux, M. Ferro, M. Sessolo, A. Williamson, D. A. Koutsouras, D. Khodagholy, M. Ramuz, X. Strakosas, R. M. Owens, C. Benar, J.-M. Badier, C. Bernard, G. G. Malliaras, *Sci. Adv.* **2015**, *1*, 1400251.
[30] D. A. Bernards, G. G. Malliaras, *Adv. Funct. Mater.* **2007**, *17*, 3538.
[31] S. Wang, M. Ha, M. Manno, C. Daniel Frisbie, C. Leighton, *Nat. Commun.* **2012**, *3*, 1210.
[32] P. Mondelli, P. Kaienburg, F. Silvestri, R. Scatena, C. Welton, M. Grandjean, V. Lemaur, E. Solano, M. Nyman, P. N. Horton, S. J. Coles, E. Barrena, M. Riede, P. Radaelli, D. Beljonne, G. N. M. Reddy, G. Morse, *J. Mater. Chem. A* **2023**, *11*, 16263.
[33] Z. Liu, F. Xue, Y. Su, Y. M. Lvov, K. Varahramyan, *IEEE Trans. Nanotechnol.* **2006**, *5*, 379.
[34] I. E. Jacobs, E. W. Aasen, J. L. Oliveira, T. N. Fonseca, J. D. Roehling, J. Li, G. Zhang, M. P. Augustine, M. Mascal, A. J. Moulé, *J. Mater. Chem. C* **2016**, *4*, 3454.

[35] C. Enengl, S. Enengl, S. Pluczyk, M. Havlicek, M. Lapkowski, H. Neugebauer, E. Ehrenfreund, *ChemPhysChem* **2016**, *17*, 3836.
[36] J. Surgailis, A. Savva, V. Druet, B. D. Paulsen, R. Wu, A. Hamidi-Sakr, D. Ohayon, G. Nikiforidis, X. Chen, I. McCulloch, J. Rivnay, S. Inal, *Adv. Funct. Mater.* **2021**, *31*, 2010165.
[37] S. Lilliu, M. Alsari, O. Bikondoa, J. E. Macdonald, M. S. Dahlem, *Sci. Rep.* **2015**, *5*, 10633.
[38] G. K. Rane, U. Welzel, S. R. Meka, E. J. Mittemeijer, *Acta Mater.* **2013**, *61*, 4524.
[39] C. Solliard, M. Flueli, *Surf. Sci.* **1985**, *156*, 487.